AIMS Materials Science, 10(3): 437–452.
DOI: 10.3934/matersci.2023024
Received: 11 February 2023
Revised: 11 May 2023
Accepted: 17 May 2023
Published: 16 June 2023

http://www.aimspress.com/journal/Materials

Research article

Evonik P25 photoactivation in the visible range by surface grafting of modified porphyrins for p-nitrophenol elimination in water

Julien G. Mahy[1,2,*], Carole Carcel[3] and Michel Wong Chi Man[3]

[1] Department of Chemical Engineering-Nanomaterials, Catalysis & Electrochemistry, University of Liège, B6a, Quartier Agora, Allée du six Août 11, 4000 Liège, Belgium
[2] Institut National de la Recherche Scientifique (INRS), Centre-Eau Terre Environnement, Université du Québec, 490, Rue de la Couronne, Québec (QC), G1K 9A9, Canada
[3] ICGM, Univ Montpellier, CNRS, ENSCM, 34095 Montpellier, France

*** Correspondence:** Email: julien.mahy@uliege.be; Tel: +3243663563.

Abstract: An Evonik P25 TiO_2 material is modified using a porphyrin containing Si-$(OR)_3$ extremities to extend its absorption spectrum in the visible range. Two different loadings of porphyrin are grafted at the surface of P25. The results show that the crystallinity and the texture of the P25 are not modified with the porphyrin grafting and the presence of the latter is confirmed by Fourier-transform infrared spectroscopy (FTIR) measurements. All three samples are composed of anatase/rutile titania nanoparticles around 20 nm in size with a spherical shape. The absorption spectra of the porphyrin modified samples show visible absorption alongside the characteristic Soret and Q bands of porphyrin, despite slightly shifted peak values. The ^{29}Si solid state nuclear magnetic resonance (NMR) spectra show that the porphyrin is linked with Ti–O–C and Ti–O–Si bonds with the Evonik P25, allowing for a direct electron transfer between the two materials. Finally, the photoactivity of the materials is assessed on the degradation of a model pollutant—*p*-nitrophenol (PNP)—in water. The degradation is substantially enhanced when the porphyrin is grafted at its surface, whereas a very low activity is evidenced for P25. Indeed, with the best sample, the activity increases from 9% to 38% under visible light illumination. This improvement is due to the activation of the porphyrin under visible light that produces electrons, which are then transferred to the TiO_2 to generate radicals able to degrade organic pollutants. The observed degradation is confirmed to be a mineralization of the PNP. Recycling experiments show a constant PNP degradation after 5 cycles of photocatalysis of 24 h each.

Keywords: photocatalysis; TiO_2; water treatment; photosensitization; grafting

1. Introduction

Water scarcity is an ever-growing concern present in many countries over the world. Water pollution is one of the main causes leading to this worldwide increasing water scarcity, alongside climate change, population growth, and intensive agriculture [1]. Pesticides discharged from farms, untreated human sewage, and industrial waste all contaminate water sources with either harmful bacteria or toxic substances, making them unsuitable for drinking or even swimming [1]. Therefore, the development of new techniques for water treatment becomes ever more urgent.

Among the methods explored so far, heterogeneous photocatalysis attracts much attention as a quaternary treatment for water to reduce micropollution [2–6]. This process uses light to activate a photocatalyst which generates radicals. More precisely, when the photocatalyst (a semiconductor material) is illuminated by photons bearing sufficient energy compared to its band gap, and photons are absorbed creating electron-hole pairs [7]. These pairs can react with species adsorbed at the surface of the material (in an aqueous medium, this is mainly with oxygen and water) to produce radicals which, in turn, react with the pollutant adsorbed on the surface of the material to induce its degradation [7–9].

TiO_2 is the most common photocatalyst [7–9], with a band gap of 3.2 eV (for its anatase phase) activated in the UV range. It has the advantage of a relatively low cost and is stable in aqueous medium. A very efficient TiO_2 photocatalyst—labeled as Evonik P25—was commercialized by the Evonik company [10], and has shown very high photoactivities for the degradation of various pollutants [10–13]. Nevertheless, this material has a poor activity under visible light exposition, especially natural solar light [14–16].

To extend the photoactivity of TiO_2 towards the visible region of light, many studies have been devoted to the modification of the structure and the composition of titania. Among these, we can cite the introduction of various dopants, modifications with metallic ions [6,17] and nanoparticles [18], non-metallic elements as N [19,20], P [21], C [22], and the combination with other semiconductors [23–25]. These modifications are usually performed during the synthesis of the TiO_2 material, thereby adding some complex preparation steps. Fortunately, some changes can be done directly on pre-synthesized TiO_2, thereby allowing for a simple modification protocol, among which include grafting photosensitizers at the surface of titania [26–32].

Among these molecules, porphyrins have shown an ability to sensitize TiO_2 towards visible light, thereby increasing its photoefficiency. Nevertheless, the bonding with TiO_2 is not always optimal, and side-effects such as leaching and photobleaching can appear [33,34].

In this paper, a modified porphyrin molecule containing Si-$(OR)_3$ extremities is grafted onto the commercial Evonik P25 TiO_2 using a very simple protocol. The physicochemical and optical properties of the modified P25 materials are then studied and the grafting mode of porphyrin on the surface is determined. In a second part of this study, the photoactivity of the resulting material is evaluated on a model pollutant *p*-nitrophenol, commonly found in pesticides. This activity is assessed under visible light and with recycling experiments. The as-received P25 material is used as a reference material throughout the entire study.

2. Materials and methods

2.1. Reagents

Evonik P25 (≥99.5%, 21 nm, Sigma-Aldrich), absolute ethanol (puriss. p.a., absolute, ≥99.8%, Sigma-Aldrich), and ultra-pure water were purchased for this study. The silylated porphyrin (structure represented on Figure S1) was obtained from the protocol fully described in [28], and contained 4 Si-$(O\text{-}Et)_3$ groups at its extremities.

2.2. Porphyrin grafting on P25

For the grafting, 1 g of Evonik P25 is stirred in 500 mL of EtOH with either 31 mg or 62 mg of silylated porphyrin for 48 h. Then, the suspension is centrifuged at 10,000 rpm for 10 min. The sample is washed in 50 mL of EtOH and then in 50 mL of ultra-pure water. The obtained samples are denoted as P25/G1 for the sample with 31 mg of porphyrin and P25/G2 for the sample with 62 mg of porphyrin. The sample denoted P25 corresponds to pure Evonik P25 TiO_2.

2.3. Characterizations

A Micromeritics ASAP 2420 analyzer is utilized to measure nitrogen adsorption–desorption isotherms at 77 K after outgassing for 24 h at ambient temperature.

X-ray diffraction-patterns are recorded using a Bruker D8 Twin-Twin powder diffractometer (Cu-K_α radiation).

UV/visible diffuse reflectance spectroscopy measurements are made on the samples with a Varian Cary 500 UV-Vis-NIR spectrophotometer, equipped with an integrating sphere (Varian External DRA-2500), and using $BaSO_4$ as a reference. The spectra are modified using the Kubelka-Munk function [35] to produce a signal and are normalized for comparison between samples. The details of this treatment method are widely described elsewhere [36].

UV/visible spectroscopy is performed on an ethanolic solution of porphyrin with a Genesys 150 UV-VIS spectrophotometer (Thermo Scientific).

Fourier transform infrared (FTIR) spectroscopy is used on the samples in the region of 500–4000 cm^{-1} with a Spectrum One FT-IR Spectrometer (PerkinElmer), performed at ambient temperature. Previously, all photocatalysts have been dispersed in KBr at 1 wt%.

Solid-state ^{29}Si NMR experiments are performed using a Bruker Avance I spectrometer at an operating 1H Larmor frequency of 400.13 MHz (B0 = 9.4 T), corresponding to a ^{29}Si Larmor frequency of 79.49 MHz. All experiments shown are obtained using a Bruker HXY 4 mm probe operating in double resonance mode, and at a magic-angle spinning (MAS) frequency of 10 kHz. ^{29}Si cross-polarization experiments are performed using a ramped-contact (50% to 100% amplitude) for a duration of 5 ms, and a recycle delay of 1s [28].

Transmission electron microscopy (TEM) is performed on a LEO 922 OMEGA Energy Filter Transmission Electron Microscope operating at 120 kV. For sample preparation, a few milligrams of each sample are dispersed in ethanol using sonication. Then, a few drops are deposited on a copper grid (CF-1.2/1.3-2 Cu-50, C-flat™, Protochips, USA) and dried at ambient temperature overnight prior to measurement acquisition.

Scanning electron microscopy (SEM) images are obtained on a field-emission scanning electron microscope JEOL 7600F operating at 15 kV.

2.4. Photocatalytic experiments

The photocatalytic activity of the samples following the degradation of *p*-nitrophenol (PNP) after 24 h is evaluated in triplicate under visible light. The experimental setup is shown in [36]. The residual concentration of PNP is measured by UV/Vis spectroscopy (GENESYS 150 UV-VIS, Thermo Scientific) at 318 nm. To assess whether complete mineralization of PNP occurs when measuring the degradation with the UV/visible spectroscopy, the samples of the photocatalytic experiments are measured using a total organic carbon analyzer (TOC-L CPN from Shimadzu).

For each experiment, the degradation percentage of PNP, D_{PNP}, is given by Eq 1:

$$D_{PNP}(\%) = \left(1 - \frac{[PNP]_i}{[PNP]_0}\right) * 100 \quad (1)$$

where $[PNP]_i$ represents the residual concentration of PNP at time t = i h and $[PNP]_0$ represents the initial concentration of PNP at time t = 0 h.

For each photocatalytic experiment, three tubes containing a photocatalyst are exposed to light to calculate PNP degradation. A blank test is made to evaluate the photolysis of PNP alone under visible light after 48 h of irradiation. Additionally, a dark test is performed to evaluate PNP adsorption on samples by keeping a test tube with PNP and photocatalyst in the dark for 24 h. In each tube, the initial concentration of photocatalyst (if present) and PNP are 1 g/L and 10^{-4} M, respectively. Experiments are conducted in test tubes fitted with a sealing cap and 10 mL of suspension under magnetic stirring.

These tubes are placed in a cylindrical glass reactor with a halogen lamp in the center. The lamp features a continuous spectrum from 300 to 800 nm (300 W, 220 V) and is covered by a UV filter to remove wavelengths lower than 400 nm (The lamp spectrum is presented in Figure S2). The reactor is maintained at a constant temperature of 20 ℃ by a cooling thermostatic bath. The lamp is also cooled by a similar system. An aluminum foil covers the outer wall of the reactor to prevent any interactions with the room lighting.

2.5. Recycling experiments

To assess the stability of the photocatalytic activity, recycling experiments are performed on the three samples. These tests consist of performing successive photocatalytic experiments on the samples with centrifugation and washing steps in between, and an ultrasonic bath is used to resuspend the photocatalysts. After 24 h of the photocatalytic test described in section 2.3, the catalysts are recovered by centrifugation (15,000 rpm for 20 min). Then, the process is repeated for another 24 h. This recycling process is made 5 successive times corresponding to 120 h of total irradiation. The fifth photocatalytic experiment on the P25/G2 sample is analyzed by TOC and compared to UV/visible spectroscopy results for PNP degradation.

3. Results and discussion

3.1. Crystallinity, texture and morphology

The X-ray diffraction (XRD) pattern for the P25 sample displays characteristic diffraction peaks of anatase and rutile phases, as expected (Figure 1) [15]. Similar patterns (not represented here) are obtained for samples grafted with porphyrin (P25/G1 and P25/G2). As grafting is a surface phenomenon, the presence of the porphyrin does not alter the crystallinity of the starting titania.

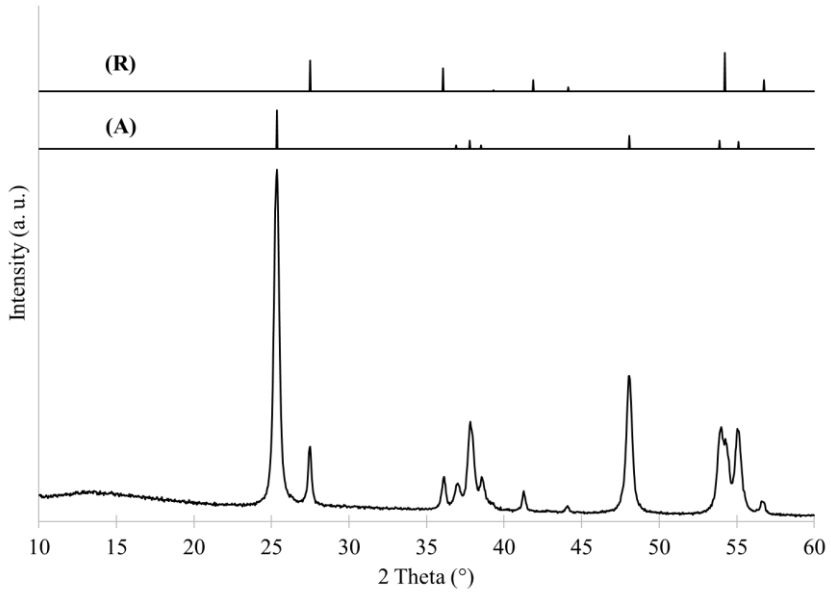

Figure 1. X-ray Diffraction (XRD) patterns of the Evonik P25 TiO_2 powder. (A) Reference pattern of anatase and (R) Reference pattern of rutile.

Figure S3 represents the nitrogen adsorption-desorption isotherm of the P25/G2 sample, which has the same shape as P25 and P25/G1. This isotherm corresponds to a type IV isotherm (microporous solids), with a hysteresis attesting the presence of mesopores [37]. The specific surface area and the micropore volume of all samples are listed in Table 1. Similar values are obtained for all the samples, suggesting that the surface grafting of porphyrin does not alter the pore texture of the starting TiO_2, as already observed in previous studies [38].

Table 1. Sample textural properties.

Sample	S_{BET} (m^2/g) ±5	V_{micro} (cm^3/g) ±0.01
P25	55	0.03
P25/G1	45	0.03
P2/G2	50	0.03

Figure 2 represents the TEM and SEM images of both P25 and P25/G2 samples. As expected, no difference can be observed between the bare and grafted samples, as only an organic molecule is

added on the surface [39]. For both samples, the characteristic morphology of P25 is found, namely spherical nanoparticles around 20 nm in diameter [39].

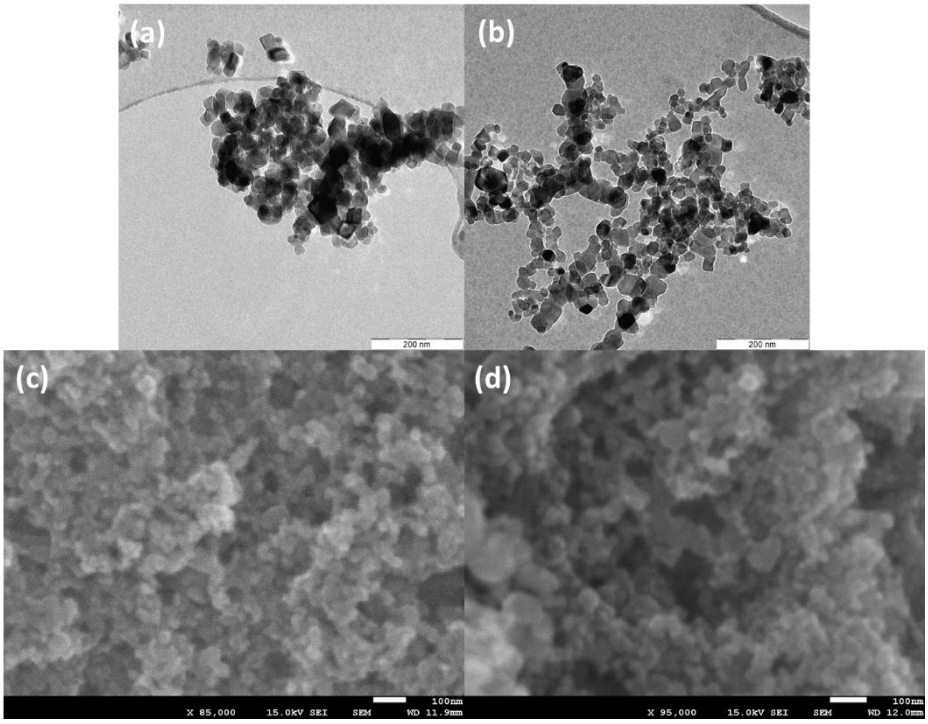

Figure 2. TEM micrographs of (a) P25 TiO_2 and (b) P25/G2 samples; and SEM images of (c) P25 TiO_2 and (d) P25/G2 samples.

3.2. Optical properties and porphyrin detection

The FTIR spectra of the porphyrin alone, P25, and P25/G2 are represented in Figure 3. When comparing the three spectra, the P25/G2 sample has a peak around 1370 cm^{-1}, corresponding to the presence of porphyrin; the other peaks observed at 3300 and between 1300 and 1700 cm^{-1} on the P25 and P25/G2 sample peaks correspond mainly to the signature of water molecules absorbed at the surface of the materials [40]. The spectrum of P25/G1 is not represented here due to its similarity to that of P25/G2, apart from a peak at 1370 cm^{-1} that is barely visible due to the lower amount of porphyrin in that sample.

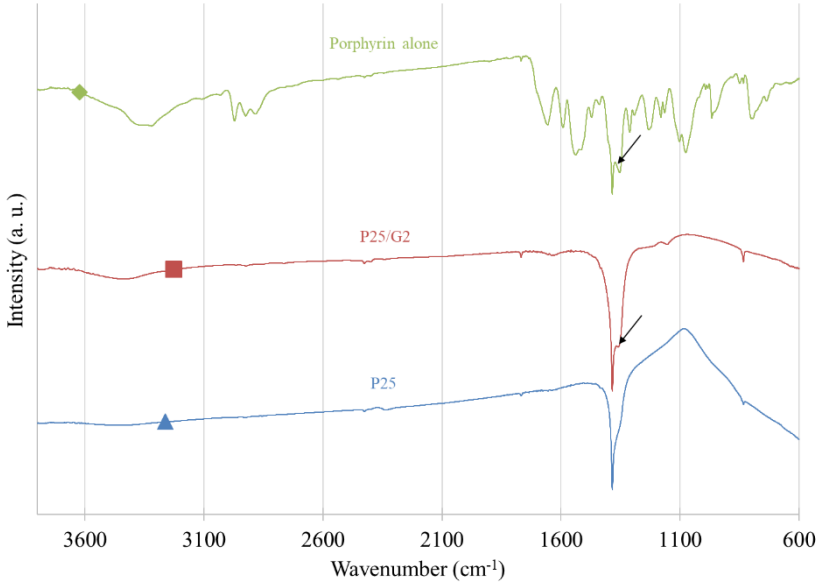

Figure 3. FTIR spectra of (▲) P25, (■) P25/G2 and (♦) porphyrin alone samples. The black arrows denote the peak around 1370 cm^{-1} characteristic of the porphyrin.

Figure 4a represents the UV/visible spectrum of the porphyrin dispersed in ethanol. Five peaks can be observed: one intense peak around 425 nm, and four less intense peaks around 517, 558, 598, and 653 nm. Those peaks correspond to the Soret band and the Q bands of porphyrin [41] and confirm that this molecule has visible light absorption.

Figure 4b shows the diffuse reflectance spectra of the P25, P25/G1, and P25/G2 samples. For P25, absorption in the UV range is observed, as expected. The two porphyrin modified samples show additional peaks corresponding to the Soret band and the Q bands of porphyrin, confirming its incorporation on the surface of the sample. The intensity of the peaks is higher in the P25/G2 sample, which contains more porphyrin, and the peaks are also much more defined in this case. Indeed, the five peaks can be clearly tagged, while for the P25/G1 sample, only the main peak is well-defined. The positions of the five peaks are around 432, 531, 570, 607, and 659 nm. Although a slight shift towards higher wavelengths is observed in this case, the result confirms the grafting of porphyrin onto the surface of P25. The energy shift can be ascribed to a slight change in the porphyrin configuration due to grafting. Given these results, it is clear that both porphyrin modified samples present absorption in visible light and in opposition to the unmodified P25.

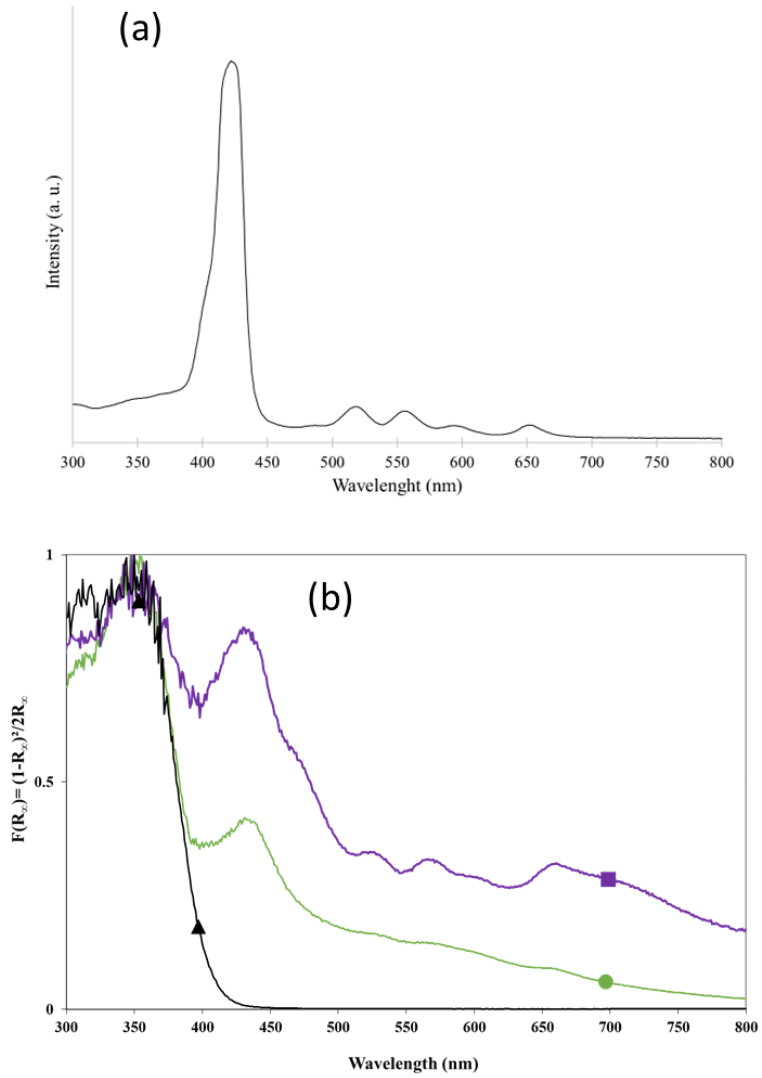

Figure 4. (a) UV/visible spectrum of an ethanolic solution of porphyrin alone and (b) Normalized Kubelka–Munk function F(R∞) calculated from diffuse reflectance UV/visible spectra for (▲) P25, (●) P25/G1, and (■) P25/G2 samples.

Figure 5 represents the solid state ^{29}Si NMR spectra of pure porphyrin and the P25/G2 sample. The spectrum of pure silylated porphyrin is characterized by a single peak located at −47 ppm, corresponding to an [R-Si-$(OR)_3$] environment surrounding the silicon atom (R denoting an organic group) [42,43]. This singlet further indicates that the molecule has not undergone any condensation.

For the P25/G2 sample, the signal to noise ratio remains low even after considerable co-added transients, demonstrating the relatively low amount of porphyrin molecules relative to the P25 TiO_2 nanoparticles. Nevertheless, three peaks can be observed at −46, −58, and −100 ppm. The peak at −46 ppm coincides with a [R-Si$(OR)_2(OTi)_1$] configuration [44], the peak at −58 ppm corresponds to a silicon site with a [R-Si-$(OR)_1(OTi)_2$] configuration [44], and the peak at −100 ppm indicates silicon (quaternary coordination oxygen) that is not bonded to the nanoparticle. The latter species may result from the formation of dimers, trimers, or higher order oligomers; an additional possibility is the bonding of the particle with a Ti-O-C link to the carbon extremities of the porphyrin [44].

From all the optical characterizations, it can be concluded that the P25/G1 and P25/G2 samples contain porphyrin grafted onto the surface of the P25 TiO_2 nanoparticles with Ti–O–Si and Ti–O–C bonding. As porphyrin is expected to provide the P25 material with a visible absorption, the samples photoactivity is evaluated in the following section.

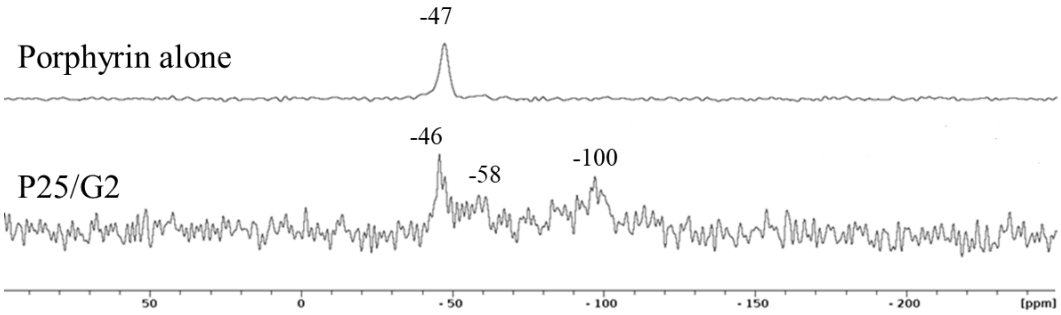

Figure 5. ^{29}Si CPMAS solid state NMR spectra of porphyrin alone and P25/G2 sample.

3.3. Photocatalytic activity under visible light

Figure 6 (light grey bars) represents the photodegradation on PNP after 24 h of illumination under visible light for the three samples. First, it is important to remind that PNP does not undergo any photolysis under visible light, since the blank test without catalyst shows no PNP degradation after 48 h of illumination. Moreover, the dark test (performed without light) shows no adsorption on the photocatalysts. Indeed, the concentration of PNP stays constant throughout the blank and dark test. The suspension of catalyst with pollutant is well-mixed thanks to magnetic stirring, and no decantation is observed for any of the three samples.

The PNP degradation with the P25 sample is very low, with only 9% of degradation after 24 h. This activity, even under visible light, may result from the fact that the UV filter used on the lamp did not completely fulfill its role, allowing a very small fraction of UV radiation to be transmitted (see Figure S2). For the two porphyrin grafted samples, the photoactivities are significantly increased with a PNP degradation of 24% and 38% for the P25/G1 and P25/G2 samples, respectively. When the modified samples are illuminated, the irradiated porphyrin is excited, transferring electrons from the HOMO to LUMO level. In turn, these electrons can be transferred to the conduction band of TiO_2 [40,45], as bonds between POR-Si and TiO_2 are observed with ^{29}Si CPMAS experiments. These transferred electrons can then react with adsorbed species (oxygen and water) to produce additional $^{\bullet}OH$ and $O_2^{-\bullet}$ radicals [46] and increase the activity of P25 TiO_2.

TOC measurements were performed to assess if the conversion measured with UV/visible spectroscopy is associated with mineralization. The results of the TOC degradation are denoted in Table 2, and are compared to the % value obtained with UV/visible spectroscopy. It is observed that the PNP degradation on the three samples is similar with both techniques. The PNP is mineralized into CO_2 and H_2O, resulting in a green depollution process that does not produce toxic by-products or release porphyrin into the medium. Indeed, concerning the use of UV/visible spectroscopy to measure the PNP degradation, it has been reported [47,48] that the presence of intermediate species associated with the partial degradation of PNP can be detected by the presence of peaks

corresponding to the intermediates (4-nitrocatechol, 1,2,4-benzenetriol, hydroquinone) in the UV/Vis spectrum measured between 250–550 nm after several hours under illumination. In the present study, the absence of supplementary peaks in the UV/Vis spectra measured between 250–550 nm is consistent with the complete mineralization of the pollutant, thereby indicating that the photocatalysts developed in this study promote the mineralization of PNP. Figure S4 shows the UV/Vis spectrum measured between 250–550 nm for the initial solution of PNP and after 24 h of illumination with the P25/G2 sample. No other peak can be noticed; therefore, when combined with the TOC measurements (Table 2), it can be concluded that mineralization occurs and that only a fraction of PNP remains after 24 h of reaction.

Figure 6 (dark grey bars) further depicts the recycling photoactivities of the three catalysts. The degradation efficiency is maintained throughout the five cycles for the porphyrin modified P25, displaying the stability of the bonds between titania and porphyrins. This stability of activity gives strength to this simple modification protocol of P25 in order to extend its activity towards a low energy visible light, which is available with the solar light. Moreover, a TOC measurement was performed on the last cycle with the best P25/G2 sample (Table 2). This measurement shows that the degradation of PNP consists of the mineralization of the molecule with a similar value as the first catalytic experiment on this sample (37% of PNP mineralization).

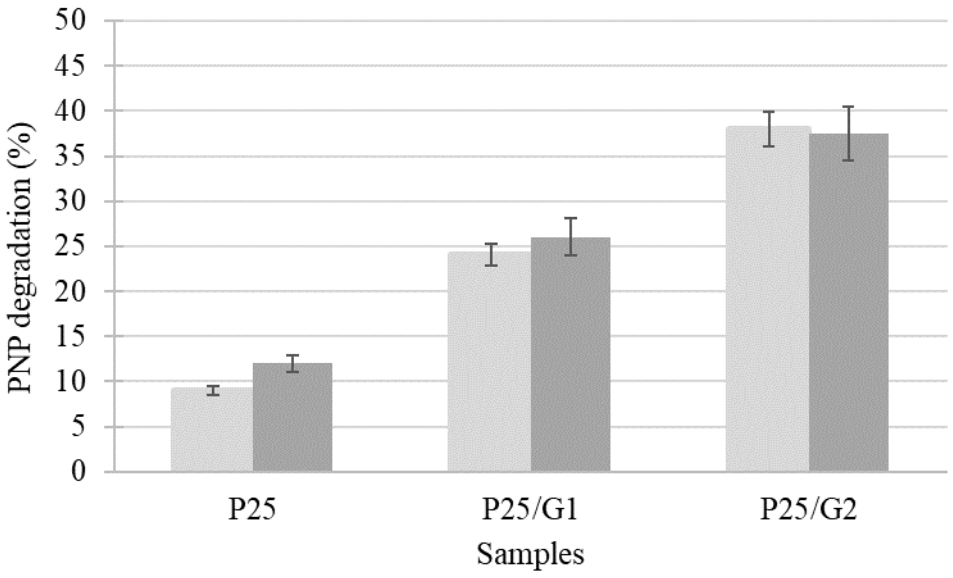

Figure 6. PNP degradation after 24 h of illumination under visible light (light grey bars) and mean PNP degradation after 5 × 24 h of illumination under visible light (dark grey bars) and recycling steps between each cycle.

Table 2. Total organic carbon (TOC) measurements after photocatalytic experiments (24 h of illumination) compared to the PNP degradation measured by UV/visible spectroscopy.

Photocatalytic experiments after 24 h of illumination	Remaining organic carbon by TOC measurements (%) ±1	PNP degradation measured by UV/visible spectroscopy (%) ±3	Remaining PNP from UV/visible spectroscopy (%) ±3	Mineralization (%)
P25	90	9	91	10
P25/G1	76	24	76	24
P25/G2	63	38	62	37
P25/G2-R5	63	37	63	37

The remaining organic carbon was calculated from the TOC measurement before and after the catalytic experiment $= \frac{TOC_{final}}{TOC_{initial}} \times 100$.

This next paragraph compares the present study to the work of Rengifo-Herrera et al. [32], where the Evonik P25 material is also modified by surface grafting to extend its activity towards the visible region of light. The main parameters of both studies are synthesized in Table 3. In Rengifo-Herrera et al. [32], P25 is modified with tungstophosphoric acid and the photocatalytic activity in the visible range is obtained on the degradation of malachite green. While [32] also modified P25 material to extend its activity towards visible range, the approach is totally different, resulting in two very different works, with described differences in the grafted molecules, the pollutant, the thermal treatment, the illumination, the doping rate, and the pollutant concentration. The work of Rengifo-Herrera et al. [32] allows for a faster conversion of the malachite green; however, the mineralization is not shown, and the concentration is ten times lower. Moreover, dyes such as malachite green undergo photobleaching, therefore making the interpretation of the photocatalytic results more difficult. Finally, it can be concluded that making a comparison is quite difficult because many conditions are completely different in these two studies, despite both advantageously contributing to the literature concerning the extension of the visible activity for the P25 material.

Table 3. Comparison of this study with the work of Rengifo-Herrera et al. [32].

Parameters for comparison	Rengifo-Herrera et al. [32]	Our study
Grafted molecule (content)	Tungstophosphoric acid (30 wt%)	Silylated porphyrin (3 & 5.8 wt%)
Thermal treatment	Calcination at 200 or 500 ℃	No calcination
Lamp used for photocatalytic experiments	Xe lamp (200–800 nm) with 3 different cut-off filters: >320, >450 and >590	Halogen lamp (300–800 nm) with a cut-off filter >390 nm
Characteristics of the photocatalytic experiments	• Pollutant (concentration): Malachite green (10^{-5} M) • Photocatalyst concentration: 1 g/L • Irradiation time: 1 h	• Pollutant (concentration): p-nitrophenol (10^{-4} M) • Photocatalyst concentration: 1 g/L • Irradiation time: 24 h
Best photocatalytic result	100% of conversion in 1 h under the cut-off filter of >450 nm	38% of mineralization in 24 h under the cut-off filter of >390 nm
Recycling experiments	No	Recycling experiments on 5 × 24 h with constant activity

4. Conclusion

In this paper, Evonik P25 TiO_2 is modified with a porphyrin containing Si-$(OR)_3$ extremities. Porphyrin is grafted onto the surface of P25 with 2 different ratios in order to extend its absorption spectrum into the visible range.

The results show that the grafting does not affect neither the crystallinity nor the texture of the P25, keeping an anatase-rutile phase material with a specific surface area around 50 m^2/g. Grafting of the porphyrin is detected with FTIR measurements, showing the characteristic peak of porphyrin at 1370 cm^{-1}. The absorption spectra of the porphyrin modified samples show visible absorption, with the characteristic Soret band and Q bands of porphyrin with a slight shift of these 5 peaks. The ^{29}Si solid state NMR spectra proves that the porphyrin is linked with Ti–O–C and Ti–O–Si bonds with the Evonik P25, allowing for a direct electron transfer between these two materials.

The photoactivity of the materials was assessed on the degradation of a model pollutant, PNP, in water. These experiments show a very low activity for bare P25, and is substantially enhanced when porphyrin is grafted at the surface. Indeed, with the best sample, P25/G2, the activity increases from 9% to 38% of PNP degradation after 24 h of illumination under visible light. This improvement of activity is due to the activation of porphyrin under visible light, which produces electrons that are transferred to TiO_2 to generate radicals able to degrade this organic pollutant into H_2O and CO_2. Recycling experiments further show the stability of both the bonds between P25 and porphyrins and its photoactivity.

Use of AI tools declaration

The authors declare they have not used Artificial Intelligence (AI) tools in the creation of this article.

Acknowledgments

Julien G. Mahy thanks the F.R.S.-FNRS for his Postdoctoral Researcher position and is furthermore grateful to the Rotary for a District 2160 grant and to the University of Liège and the FNRS for their financial support for a postdoctoral stay in INRS Centre eau, terre, environnement in Québec, Canada. The authors thank the CARPOR platform from the University of Liège for the pore texture characterization of the catalysts and Ir. Bruno Correia and Dr. Alexandre Léonard for their revisions of the manuscript.

Conflict of Interest

The authors declare that there is no conflict of interest concerning this work.

Reference

1. Turolla A, Fumagalli M, Bestetti M, et al. (2012) Electrophotocatalytic decolorization of an azo dye on TiO_2 self-organized nanotubes in a laboratory scale reactor. *Desalination* 285:377–382. https://doi.org/10.1016/j.desal.2011.10.029
2. Oturan MA, Aaron JJ (2014) Advanced oxidation processes in water/wastewater treatment: Principles and applications. A review. *Crit Rev Environ Sci Technol* 44: 2577–2641. https://doi.org/10.1080/10643389.2013.829765
3. Mahy JG, Wolfs C, Mertes A, et al. (2019) Advanced photocatalytic oxidation processes for micropollutant elimination from municipal and industrial water. *J Environ Manage* 250: 109561. https://doi.org/10.1016/j.jenvman.2019.109561
4. Mahy JG, Wolfs C, Vreuls C, et al. (2021) Advanced oxidation processes for wastewater treatment: From lab-scale model water to on-site real waste water. *Environ Technol* 42: 3974–3986. https://doi.org/10.1080/09593330.2020.1797894
5. Baaloudj O, Nasrallah N, Kebir M, et al. (2021) A comparative study of ceramic nanoparticles synthesized for antibiotic removal: catalysis characterization and photocatalytic performance modeling. *Environ Sci Pollut R* 28: 13900–13912. https://doi.org/10.1007/s11356-020-11616-z/Published
6. Baaloudj O, Nasrallah N, Bouallouche R, et al. (2022) High efficient Cefixime removal from water by the sillenite $Bi1_2TiO_{20}$: Photocatalytic mechanism and degradation pathway. *J Clean Prod* 330: 12994. https://doi.org/10.1016/j.jclepro.2021.129934
7. Fujishima A, Hashimoto K, Watanabe T (1999) *TiO_2 Photocatalysis: Fundamentals and Applications*, BKC.
8. Rauf MA, Ashraf SS (2009) Fundamental principles and application of heterogeneous photocatalytic degradation of dyes in solution. *Chem Eng J* 151: 10–18. https://doi.org/10.1016/j.cej.2009.02.026
9. Mahy JG, Léonard GL-M, Pirard S, et al. (2017) Aqueous sol-gel synthesis and film deposition methods for the large-scale manufacture of coated steel with self-cleaning properties. *J Sol-gel Sci Technol* 81: 27–35. https://doi.org/10.1007/s10971-016-4020-5

10. Malengreaux CM, Douven S, Poelman D, et al. (2014) An ambient temperature aqueous sol-gel processing of efficient nanocrystalline doped TiO_2-based photocatalysts for the degradation of organic pollutants. *J Sol-gel Sci Technol* 71: 557–570. https://doi.org/10.1007/s10971-014-3405-6
11. Todorova N, Giannakopoulou T, Karapati S, et al. (2014) Composite TiO_2/clays materials for photocatalytic NOx oxidation. *Appl Surf Sci* 319: 113–120. https://doi.org/10.1016/j.apsusc.2014.07.020
12. Romeiro A, Azenha ME, Canle M, et al. (2018) Titanium dioxide nanoparticle photocatalysed degradation of ibuprofen and naproxen in water: Competing hydroxyl radical attack and oxidative decarboxylation by semiconductor holes. *ChemistrySelect* 3: 10915–10924. https://doi.org/10.1002/slct.201801953
13. Mbouopda AP, Acayanka E, Nzali S, et al. (2018) Comparative study of plasma-synthesized and commercial-P25 TiO_2 for photocatalytic discoloration of reactive Red 120 dye in aqueous solution. *Desalination Water Treat* 136: 413–421. https://doi.org/10.5004/dwt.2018.23118
14. Mahy JG, Tilkin RG, Douven S, et al. (2019) TiO_2 nanocrystallites photocatalysts modified with metallic species: Comparison between Cu and Pt doping. *Surf Interface* 17: 100366. https://doi.org/10.1016/j.surfin.2019.100366
15. Mahy JG, Lambert SD, Tilkin RG, et al. (2019) Ambient temperature ZrO_2-doped TiO_2 crystalline photocatalysts: Highly efficient powders and films for water depollution. *Mater Today Energy* 13: 312–322. https://doi.org/10.1016/j.mtener.2019.06.010
16. Douven S, Mahy JG, Wolfs C, et al. (2020) Efficient N, Fe Co-doped TiO_2 active under cost-effective visible LED light: From powders to films. *Catalysts* 10: 547. https://doi.org/10.3390/catal10050547
17. Impellizzeri G, Scuderi V, Romano L, et al. (2016) Fe ion-implanted TiO_2 thin film for efficient visible-light photocatalysis Fe ion-implanted TiO_2 thin film for efficient visible-light photocatalysis. *J Appl Phys* 116: 173507. https://doi.org/10.1063/1.4901208
18. Espino-estévez MR, Fernández-rodríguez C, González-díaz OM (2016) Effect of TiO_2-Pd and TiO_2-Ag on the photocatalytic oxidation of diclofenac, isoproturon and phenol. *Chem Eng J* 298: 82–95. https://doi.org/10.1016/j.cej.2016.04.016
19. Mahy JG, Cerfontaine V, Poelman D, et al. (2018) Highly efficient low-temperature N-doped TiO_2 catalysts for visible light photocatalytic applications. *Materials* 11: 584. https://doi.org/10.3390/ma11040584
20. Pelaez M, Nolan NT, Pillai SC, et al. (2012) A review on the visible light active titanium dioxide photocatalysts for environmental applications. *Appl Catal B* 125: 331–349. https://doi.org/10.1016/j.apcatb.2012.05.036
21. Bodson CJ, Heinrichs B, Tasseroul L, et al. (2016) Efficient P- and Ag-doped titania for the photocatalytic degradation of wastewater organic pollutants. *J Alloys Compd* 682: 144–153. https://doi.org/10.1016/j.jallcom.2016.04.295
22. Léonard GLM, Remy S, Heinrichs B (2016) Doping TiO_2 films with carbon nanotubes to simultaneously optimise antistatic, photocatalytic and superhydrophilic properties. *J Sol-gel Sci Technol* 79: 413–425. https://doi.org/10.1007/s10971-016-3975-6
23. Léonard GL-M, Pàez CA, Ramírez AE, et al. (2018) Interactions between Zn^{2+} or ZnO with TiO_2 to produce an efficient photocatalytic, superhydrophilic and aesthetic glass. *J Photochem Photobiol A Chem* 350. https://doi.org/10.1016/j.jphotochem.2017.09.036

24. Reinosa JJ, María C, Docio Á, et al. (2018) Hierarchical nano ZnO-micro TiO_2 composites: High UV protection yield lowering photodegradation in sunscreens. *Ceram Int* 44: 2827–2834. https://doi.org/10.1016/j.ceramint.2017.11.028
25. Wu M, Leung DYC, Zhang Y, et al. (2019) Toluene degradation over Mn-TiO_2/CeO_2 composite catalyst under vacuum ultraviolet (VUV) irradiation. *Chem Eng Sci* 195: 985–994. https://doi.org/10.1016/j.ces.2018.10.044
26. Min KS, Kumar RS, Lee JH, et al. (2019) Synthesis of new TiO_2/porphyrin-based composites and photocatalytic studies on methylene blue degradation. *Dyes and Pigments* 160: 37–47. https://doi.org/10.1016/j.dyepig.2018.07.045
27. Wu T, Lin T, Serpone N (1999) TiO_2-assisted photodegradation of dyes. 9. photooxidation of a squarylium cyanine dye in aqueous dispersions under visible light irradiation. *Environ Sci Technol* 33:1379–1387. https://doi.org/10.1021/es980923i
28. Mahy JG, Paez CA, Carcel C, et al. (2019) Porphyrin-based hybrid silica-titania as a visible-light photocatalyst. *J Photochem Photobiol A Chem* 373: 66–76. https://doi.org/10.1016/j.jphotochem.2019.01.001
29. Musial J, Belet A, Mlynarczyk DT, et al. (2022) Nanocomposites of titanium dioxide and peripherally substituted phthalocyanines for the photocatalytic degradation of sulfamethoxazole. *Nanomaterials* 12: 3279. https://doi.org/10.3390/nano12193279
30. Ramasubbu V, Ram Kumar P, Chellapandi T, et al. (2022) Zn(II) porphyrin sensitized (TiO_2@Cd-MOF) nanocomposite aerogel as novel photocatalyst for the effective degradation of methyl orange (MO) dye. *Opt Mater*132: 112558. https://doi.org/10.1016/j.optmat.2022.112558
31. Yadav V, Verma P, Negi H, et al. (2023) Efficient degradation of 4-nitrophenol using VO(TPP) impregnated TiO_2 photocatalyst: Insight into kinetics and mechanism. *J Mater Res* 38: 237–247. https://doi.org/10.1557/s43578-022-00856-z
32. Rengifo-Herrera JA, Blanco MN, Fidalgo De Cortalezzi MM, et al. (2016) Visible-light-absorbing Evonik P-25 nanoparticles modified with tungstophosphoric acid and their photocatalytic activity on different wavelengths. *Mater Res Bull* 83: 360–368. https://doi.org/10.1016/j.materresbull.2016.06.026
33. Wang L, Duan S, Jin P, et al. (2018) Anchored Cu(II) tetra(4-carboxylphenyl)porphyrin to P25 (TiO_2) for efficient photocatalytic ability in CO_2 reduction. *Appl Catal B* 239: 599–608. https://doi.org/10.1016/j.apcatb.2018.08.007
34. Tio N, Cherian S, Wamser CC (2000) Adsorption and photoactivity of tetra (4-carboxyphenyl) porphyrin (TCPP) on nanoparticulate TiO_2. *J Phys Chem B* 104: 3624–3629. https://doi.org/10.1021/jp994459v
35. Kubelka P (1948) New contributions to the optics of intensely light-scattering materials. *J Opt Soc Am* 38:448–457. https://doi.org/10.1364/JOSA.44.000330
36. Mahy JG, Lambert SD, Léonard GLM, et al. (2016) Towards a large scale aqueous sol-gel synthesis of doped TiO_2: Study of various metallic dopings for the photocatalytic degradation of p-nitrophenol. *J Photochem Photobiol A Chem* 329: 189–202. https://doi.org/10.1016/j.jphotochem.2016.06.029
37. Thommes M, Kaneko K, Neimark A, et al. (2015) Physisorption of gases, with special reference to the evaluation of surface area and pore size distribution (IUPAC Technical Report). *Pure Appl Chem* 87: 1051–1069. https://doi.org/10.1515/pac-2014-1117

38. Tasseroul L, Páez CA, Lambert SD, et al. (2016) Photocatalytic decomposition of hydrogen peroxide over nanoparticles of TiO_2 and Ni(II)porphyrin-doped TiO_2: A relationship between activity and porphyrin anchoring mode. *Appl Catal B* 182: 405–413. https://doi.org/10.1016/j.apcatb.2015.09.042
39. Mahy JG, Douven S, Hollevoet J, et al. (2021) Easy stabilization of Evonik Aeroxide P25 colloidal suspension by 4-hydroxybenzoic acid functionalization. *Surf Interface* 27: 101501. https://doi.org/10.1016/j.surfin.2021.101501
40. Tasseroul L, Lambert SD, Eskenazi D, et al. (2013) Degradation of p-nitrophenol and bacteria with TiO_2 xerogels sensitized in situ with tetra(4-carboxyphenyl) porphyrins. *J Photochem Photobiol A Chem* 272: 90–99. https://doi.org/10.1016/j.jphotochem.2013.08.023
41. Tasseroul L, Pirard SL, Lambert SD, et al. (2012) Kinetic study of p-nitrophenol photodegradation with modified TiO_2 xerogels. *Chem Eng J* 191: 441–450. https://doi.org/10.1016/j.cej.2012.02.050
42. Cerneaux S, Zakeeruddin SM, Pringle JM, et al. (2007) Novel nano-structured silica-based electrolytes containing quaternary ammonium iodide moieties. *Adv Funct Mater* 17: 3200–3206. https://doi.org/10.1002/adfm.200700391
43. Corriu RJP, Moreau JJE, Thepot P, et al. (1992) New mixed organic-inorganic polymers: Hydrolysis and polycondensation of bis(trimethoxysilyl) organometallic precursors. *Chem Mater* 4: 1217–1224. https://doi.org/10.1021/cm00024a020
44. Chan Y-J, Kum B-G, Park Y-C, et al. (2014) Surface modification of TiO_2 nanoparticles with phenyltrimethoxysilane in dye-sensitized solar cells. *Bull Korean Chem Soc* 35: 415–418. https://doi.org/10.5012/bkcs.2014.35.2.415
45. Kathiravan A, Renganathan R, Anandan S (2010) Electron transfer dynamics from the singlet and triplet excited states of meso-tetrakis (p-carboxyphenyl) porphyrin into colloidal. *J Colloid Interface Sci* 348: 642–648. https://doi.org/10.1016/j.jcis.2010.05.002
46. Baaloudj O, Assadi AA, Azizi M, et al. (2021) Synthesis and characterization of $ZnBi_2O_4$ nanoparticles: Photocatalytic performance for antibiotic removal under different light sources. *Appl Sci-Basel* 11: 3975. https://doi.org/10.3390/app11093975
47. Paola A Di, Augugliaro V, Palmisano L, et al. (2003) Heterogeneous photocatalytic degradation of nitrophenols. *J Photochem Photobiol A Chem* 155: 207–214. https://doi.org/10.1016/S1010-6030(02)00390-8
48. Augugliaro V, Palmisano L, Schiavello M, et al. (1991) Photocatalytic degradation of nitrophenols in aqueous titanium dioxide dispersion. *Appl Catal* 69: 323–340. https://doi.org/http://dx.doi.org/10.1016/S0166-9834(00)83310-2